A HYBRID SCHEME TO COMPUTE CONTACT DISCONTINUITIES IN ONE-DIMENSIONAL EULER SYSTEMS

Thierry Gallouët, Jean-Marc Hérard, Nicolas Seguin

A HYBRID SCHEME TO COMPUTE CONTACT DISCONTINUITIES IN EULER SYSTEMS

THIERRY GALLOUËT*, JEAN-MARC HÉRARD*†, AND NICOLAS SEGUIN*†

Abstract. The present paper is devoted to the computation of single phase or two phase flows using the single-fluid approach. Governing equations rely on Euler equations which may be supplemented by conservation laws for mass species. Emphasis is given on numerical modelling with help of Godunov scheme or an approximate form of Godunov scheme called VFRoe-ncv based on velocity and pressure variables. Three distinct classes of closure laws to express the internal energy in terms of pressure, density and additional variables are exhibited. It is shown first that standard conservative formulation of above mentionned schemes enables to predict "perfectly" unsteady contact discontinuities on coarse meshes, when the EOS belongs to the first class. On the basis of previous work issuing from literature, an almost conservative though modified version of the scheme is proposed to deal with EOS in the second or third class. Numerical evidence shows that the accuracy of approximations of discontinuous solutions of standard Riemann problems is strenghtened on coarse meshes, but that convergence towards the right shock solution may be lost in some cases involving complex EOS in the third class. Hence, a blend scheme is eventually proposed to benefit from both properties ("perfect" representation of contact discontinuities on coarse meshes, and correct convergence on finer meshes). Computational results based on an approximate Godunov scheme are provided and discussed.

Key words. Godunov scheme, Euler system, contact discontinuities, thermodynamics, conservative schemes

1. Introduction. Computation of gas-liquid flows is of great importance in several industrial fields. For instance, when focusing on nuclear safety problems, two great problems arise. The first one is known as the LOCA (Loss Of Coolant Accident) problem. It corresponds to the unsteady flow of highly pressurised water entering an open domain initially occupied by still air at atmospheric pressure. The resulting flow contains a mixture of water and air, and the thermodynamical behaviour of the medium is quite uneasy to describe and therefore to compute. Another problem corresponds to the ebullition crisis, due to sudden heating of coolant in reactor. The flow suddenly becomes highly unsteady and contains two phases (liquid water for instance and saturated vapour). The dynamics of the whole is not very well understood up to now, both from a dynamical point of view and thermodynamical aspect.

Simple models may be proposed in order to try to account for the physics involved in these problems. The most well known is the Homogeneous Equilibrium Model. It only (!) requires to give a suitable EOS. This one may be very simple or much more complex and tabulated [38]. It nonetheless requires Euler type solvers which enable computing strong rarefaction waves, shocks and contact discontinuities. Many schemes have been proposed to deal with that kind of system with reasonable success [6], [16], [13], [47], [14], which rely on "standard" upwinding techniques such as those developed to cope with aerodynamics [22], [46], [39], [23], [45], [36], ... Another physically relevant approach relies on the Homogeneous Relaxation Model, which in addition requires computing an extra mass balance equation including (stiff) source terms in order to account for mass transfer terms between phases (see for instance the work of Bilicki and co-workers [9], [8], [7]). More complex models may also be suggested to predict two phase flow patterns on the basis of the two fluid approach for

*LATP-UMR CNRS 6632, CMI, Université de Provence, 39 rue Joliot Curie, 13453 Marseille cedex 13, France (gallouet@cmi.univ-mrs.fr, herard@cmi.univ-mrs.fr).

†Département MFTT, Électricité de France - R. et D., 6 quai Watier, 78401 Chatou cedex, France (herard@chi80bk.der.edf.fr, seguin@chi80bk.der.edf.fr).

instance [27], using the single pressure or the two pressure approach [47], [41], [21]. These *a fortiori* require better understanding of physical process involved but also urge the development of stable and highly accurate algorithms, due to the occurence of many different time scales, and to other specific problems including presence of first order non conservative terms and of stiff source terms, conditional hyperbolicity when retaining the single pressure approach, ... Actually similar (and even more complex) problems arise which confirm the need for accurate prediction of contact discontinuities.

Restricting here our attention to the frame of the single fluid approach and Euler type systems, it is now well known that great difficulties in computations arise when attempting at computing shock tube test cases with high pressure ratio and distinct phases on each side of the initial membrane. Part of the difficulty is connected with the need to compute the contact discontinuity with sufficient accuracy. This has already been pointed out in the literature by different workers including Karni [29], [30], Abgrall [1] for instance. It clearly appears in preliminary computations that fully conservative schemes such as Godunov scheme provide rather poor accuracy around contact discontinuities, when the EOS is not the basic single component perfect gas EOS, when examinating coarse meshes. This is a particularly annoying point when one aims at providing an *a posteriori* computation of a discrete gradient of the ratio $T = P/\rho$, which of course requires sufficient accuracy close to the contact discontinuity. Another point which urges for a global effort in this direction is connected with the very small rate of convergence of variables governed by pure advection, say:

$$\frac{\partial g}{\partial t} + U\frac{\partial g}{\partial x} = 0, \tag{1.1}$$

the measure of which is provided for instance in [18], and is approximately $\frac{1}{2}$ for so called first-order schemes, and $\frac{2}{3}$ for so called second-order schemes, when the initial data is discontinuous. Figure 1.1 provides a measure of the error in L^1 norm when computing a pure contact discontinuity of the Euler system of gas dynamics with perfect gas state law.

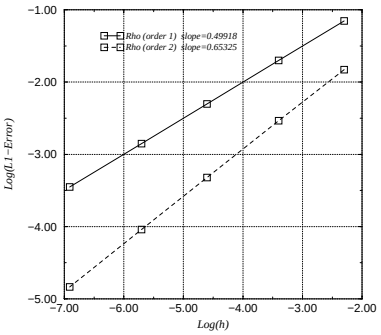

FIG. 1.1. *L1 norm of the error. Moving contact discontinuity in Euler system (perfect gas EOS)*

Actually, several ways to tackle with the problem of moving contact discontinuities have been suggested by Karni [29], [30], Abgrall [1], Karni and Abgrall [31], Fedkiw, Aslam , Merriman and Osher [17], Sethian [43], Saurel and Abgrall [42], and other workers Shyue [44], Allaire, Clerc and Kokh [3], [4], [33], Lagoutière [34], Barberon, Helluy and Rouy [5],.....

We note anyway that focus has actually been given on specific EOS such as mixture of perfect gases, or equivalently to stiffened gas EOS. More recently Van der Waals EOS has been investigated by Shyue ([44]). In the latter case, the difference between the physical model, namely the set of PDE with adequate initial and boundary conditions, and the number of discrete equations which is computed, is not totally clear. More precisely, the exact amount of redundent discrete information, and the specificities due to particular choice of EOS, or of basic flux schemes in the fully conservative schemes, do not clearly arise. In the approach proposed below, it will be seen for instance that the choice of stiffened gas EOS is quite different from the choice of Van der Waals EOS.

The purpose of the present paper is thus the following. It is intended to provide some generic way to compute accurately Euler type systems on coarse meshes and on fine meshes with help of Godunov scheme at least, and if possible with cheaper algorithms in order to cope with the broadest frame of equations of state. Since no theoretical result on convergence is reachable, it seems also of great interest to:

1. provide numerical evidence that the basic Godunov scheme and a sufficiently broad class of approximate Godunov schemes converge for any EOS towards the right solution,
2. examine whether modified "Godunov" schemes converge towards the right solution.

The presently proposed strategy enables to deal with any EOS, in such a way that schemes remain fully conservative (in terms of mass, momentum and total energy) for a basic class of EOS including the perfect gas EOS for single component flows. For complex EOS, it only requires computing one (or two) extra equations (indeed *redundent* discrete information), depending on the specific form of the EOS. From a practical point of view, one only needs to decompose the EOS in order to distinguish contributions pertaining to three distinct classes. The first class is perfectly accounted for by standard schemes, when defining discrete pressure as the analytical value of pressure $P(\rho, e, C, \psi)$ in terms of conservative variables only, using standard definitions: $U_i^n = Q_i^n/\rho_i^n$ ($Q = \rho U$ is the momentum), $e_i^n = (E_i^n - \frac{1}{2}\rho_i^n U_i^n U_i^n)/\rho_i^n$, $C_i^n = (\rho C)_i^n/\rho_i^n$ and either ψ_i^n when the colour function is computed with a non conservative equation, or its counterpart $\psi_i^n = (\rho\psi)_i^n/\rho_i^n$ in the conservative case. The second class contains EOS such as the mixture of perfect gases, the stiffened gas EOS, and similar laws, and the third one the remaining. *If an extra equation needs to be computed, it is only used to express the discrete value of the pressure at the end of any time step in terms of conservative variables, and additional redundent information, in order to compute the Riemann problems on cell interfaces at the beginning of the time step.* Throughout the paper we shall call p_i^n the pressure on cell i at time $n\Delta t$ which is used to compute local one dimensional Riemann problem at each interface, and:

$$P_i^n = P(\rho_i^n, e_i^n, C_i^n, \psi_i^n) \tag{1.2}$$

the pressure given by the EOS (thus given by a analytic or tabulated law).

The paper will be organised as follows. We will first briefly recall the governing set of equations of the single-phase or two-phase model assuming equal velocities within each phase. Closure laws to express internal energy in terms of pressure, density and (possibly) complementary variables including concentrations of species will be detailed, and three distinct classes of EOS will be exhibited. Restricting then to

the exact Godunov scheme to deal with conservation laws, or in an alternative way to an approximate Godunov scheme called VFRoe-ncv which is based on velocity and pressure variables ([11], [18], [20]), a modified version of the basic fully conservative scheme is proposed in order to improve accuracy of computations on coarse meshes (a short presentation of VFRoe-ncv schemes is provided in appendix). We emphasize that an important ingredient in the method proposed below is that the *interface Riemann solver* perfectly preserves unsteady contact discontinuities. As a result, we will focus on either the exact Godunov solver, or on approximate Godunov solvers such as those described in [11], [18], [20]. Results obtained when computing a single component perfect gas state law, a mixture of perfect gases, Van der Waals EOS are discussed first. The latter three belong to the three distinct classes. Numerical techniques have already been proposed in the literature to give accurate representation of unsteady contact discontinuities on coarse meshes, and it will be shown that the whole approach exactly corresponds the one previously proposed by Abgrall, Karni, Saurel and Shyue. Other computations including EOS with Chemkin database, and any tabulated EOS will be eventually discussed, which again will confirm that accurate approximations of solutions of shock tube experiments may be obtained with any kind of EOS, even when these have some non negligible contribution in the thrid class.

We emphasize that though somewhat similar, the present approach should not be confused with the efficient energy relaxation method proposed by Coquel and Perthame (see [15] and also [26], [25]).

2. Governing equations. The governing set of equations takes the form:

$$\left\{ \begin{array}{l} \dfrac{\partial W}{\partial t} + \dfrac{\partial F(W)}{\partial x} = 0, \\ W(0,x) = W_0(x), \end{array} \right. \tag{2.1}$$

with W, $F(W)$ with values in $\mathbb{R}^5$. The conservative variable W and convective flux $F(W)$ read:

$$\begin{array}{l} W^t = (\rho, \rho C, \rho U, E, \rho\psi), \\ F(W)^t = (\rho U, \rho C U, \rho U^2 + P, U(E+P), \rho\psi U), \end{array} \tag{2.2}$$

The total energy is written in terms of the kinetic energy plus the internal energy ρe which depends on density ρ and pressure P, but may also depend on concentration C and colour function ψ. Thus:

$$E = \frac{\rho U^2}{2} + \rho e(P, \rho, C, \psi) \tag{2.3}$$

The governing equation for the colour function is more commonly written in non conservative form $\partial_t \psi + U \partial_x \psi = 0$. We nonetheless will priviledge the conservative form in order to remove any ambiguity concerning formulation of jump conditions. This equation on colour function is useful in some cases, for instance when modeling stiffened gas EOS. The whole must be complemented with a physically relevant entropy inequality:

$$\frac{\partial \eta}{\partial t} + \frac{\partial F_\eta}{\partial x} \leq 0 \tag{2.4}$$

We introduce the speed of density waves c following: $\rho c^2 = (P/\rho - \rho \partial e/\partial \rho)(\partial e/\partial P)^{-1}$ (recall that e is a function of P, ρ, C, ψ). We assume that $gammaP = \rho c^2$ is positive.

Thus the system is hyperbolic. It has real eigenvalues and associated right eigenvectors span the whole space $\mathbb{R}^5$. Eigenvalues are:

$$\lambda_1 = U - c, \lambda_2 = \lambda_3 = \lambda_4 = U, \lambda_5 = U + c \tag{2.5}$$

The specific entropy s complies with $\hat{\gamma} P \frac{\partial s(P,\rho,C,\psi)}{\partial P} + \rho \frac{\partial s(P,\rho,C,\psi)}{\partial \rho} = 0$.
The 1 and 5-fields are Genuinely Non Linear [45], and the $2-3-4$-field is Linearly Degenerated, since:

$$\nabla_W \lambda_2(W).r_2(W) = \nabla_W \lambda_3(W).r_3(W) = \nabla_W \lambda_4(W).r_4(W) = 0 \tag{2.6}$$

Whatever the EOS is, both the pressure and the velocity are Riemann invariants in the three Linearly Degenerate fields. Jump conditions simply write (σ stands for the speed of the discontinuity):

$$-\sigma[W] + [F(W)] = 0 \tag{2.7}$$

Using some basic algebra, one gets the following counterpart:

$$\begin{array}{c} v = U - \sigma \\ \rho v[v] + [P] = 0 \\ [\rho v] = 0 \\ \rho v[(e + \frac{P}{\rho} + \frac{v^2}{2})] = 0 \\ \rho v[C] = 0 \\ \rho v[\psi] = 0 \end{array} \tag{2.8}$$

We also briefly recall the list of Riemann invariants in the 1-rarefaction wave (respectively the 5-rarefaction wave) are $I_1 = \{s, U + \int_0^\rho (c(\rho, s, C, \psi)/\rho) d\rho, \psi, C\}$ (respectively $I_5 = \{s, U - \int_0^\rho (c(\rho, s, C, \psi)/\rho) d\rho, \psi, C\}$). Details on computation of specific entropy are recalled in appendix B of [19]. Note also that: $I_{2,3,4} = \{P, U\}$.

3. Equation Of State. *The next sections are dedicated to EOS which are such that the internal energy may be expressed in terms of some analytic function of the unknowns. The specific case where thermodynamical coefficients issue from tabulated laws will be discussed in a next section.*

We now introduce three distinct classes of EOS. The first one, which is noted T_1, contains EOS which agree with:

$$\rho e = \phi_1(P, \rho, C, \psi) = \rho(a_1(P) + b_1(P)C + c_1(P)\psi) + d_1(P) \tag{3.1}$$

The second class contains EOS which *do not lie* in T_1 but nevertheless agree with:

$$\rho e = \phi_2(P, C, \psi) = f_2(C, \psi)h_2(P) + g_2(C, \psi) \tag{3.2}$$

where both f_2 and g_2 should differ from constants. The third class T_3 contains *the remaining.*

Note first that for given pressure $P = P_{ref}$, the function $\phi_1(P_{ref}, \rho, C, \psi)$ is *linear* w.r.t. unknowns ρ, ρC and $\rho\psi$. This has important consequences as will be discussed later. Note for instance that Tamman EOS, single component perfect gas EOS belong to the first class. It also includes EOS such as Tait EOS for solid material (see for instance [28]).

The second class contains laws such as the stiffened gas EOS ([42], [41], [40]):

$$\rho e = \frac{P - P_\infty(\psi)}{\gamma(\psi) - 1}$$

and the mixture of perfect gases ([1]):

$$\rho e = \frac{P}{\gamma(C) - 1}.$$

Note of course that Van der Waals EOS [35]:

$$\begin{aligned} \rho e &= \rho C_v T - a(\rho)^2, \\ (P + a(\rho)^2)(1 - b\rho) &= \rho RT \end{aligned}$$

does not belong to the latter two, nor does Mie-Gruneisen EOS (unless of course in some degenerated cases where they identify with previous mentionned laws, given specific (say null) values of constants imbeded). Obviously complex laws such as those described in [37], [32] are in T_3.

4. Properties of Godunov type schemes with any EOS. *All results in the present section are independent of the kind of EOS application.* Let Φ be a regular function from $\mathbb{R}^5$ to $\mathbb{R}^5$ and Ψ its inverse (we use the notation $Y = \Phi(W)$). Schemes used herein take the form:

$$h_i(W_i^{n+1} - W_i^n) + \delta t(F(\Psi(Y^*_{i+1/2})) - F(\Psi(Y^*_{i-1/2}))) = 0 \tag{4.1}$$

where h_i and δt respectively denote the mesh size and the time step chosen in agreement with a CFL condition, W_i^n stands for the mean value of conservative variable W over cell i at time t_n, and $Y^*_{i+1/2}$ is the exact (or approximate) value of the associated Riemann problem at the interface between two neighbouring cells with associated cell values $\Phi(W_i^n)$ and $\Phi(W_{i+1}^n)$. This provides updated value of conservative variable W_i^{n+1}, which enables to get the natural "obvious" definition of e_i^n:

$$\rho_i^n e_i^n = E_i^n - \frac{1}{2}\rho_i^n U_i^n U_i^n \tag{4.2}$$

and standard definitions: $U_i^n = Q_i^n/\rho_i^n$, $C_i^n = (\rho C)_i^n/\rho_i^n$, (and if required $\psi_i^n = (\rho\psi)_i^n/\rho_i^n$). Hence, one may then extract P_i^n as the value of the function P (given by the EOS) for given arguments ρ_i^n, e_i^n, C_i^n (and if required ψ_i^n), and we set here:

$$p_i^n = P_i^n \tag{4.3}$$

where P_i^n issues from (1.2). It is emphasized here that this "natural" definition of p_i^n will be modified in the next sections which deal with EOS in $T_2 \cup T_3$.We recall that due to the specific form of the governing equations, both C and ψ are Riemann invariants through the 1 -field and the 5 -field. Evenmore, assuming that these Genuinely Non Linear fields contain some discontinuity, we still have: $[C] = [\psi] = 0$. Now:

PROPERTY 4.1. *Assume that we use either the exact Godunov scheme or some approximate Godunov scheme such as VFRoe-ncv scheme (see appendix, or [11], [18], [20]) in terms of* $Y^t = (U, P, g(\rho, s), C, \psi)$. *Intermediate states indexed* Y_l *and* Y_r *agree with:*

$$\begin{aligned} C_L &= C_l, & C_r &= C_R, \\ \psi_L &= \psi_l, & \psi_r &= \psi_R, \\ U_l &= U_r, & P_l &= P_r, \end{aligned}$$

given left and right initial states $Y_L = \Phi(W_L)$ *and* $Y_R = \Phi(W_R)$.

For practical applications, we either use function $g(\rho, s) = 1/\rho$ (see [10], [11]), or $g(\rho, s) = \rho$ – in that case, the scheme is close to PVRS scheme proposed by Toro [46] – , or $g(\rho, s) = s$ in order to cope with vacuum ([20]). Recall that variable $Y^t = (U, P, s, C, \psi)$ enables to symmetrize the system. A detailed comparison of performances of VFRoe-ncv scheme with other well-known schemes is available in [18]. The proof is straightforward for Godunov scheme, and very easy for VFRoe-ncv scheme (see [18]). On this basis, we also obviously check that for both solvers mentionned above, the following holds:

PROPERTY 4.2. *Assume that the initial condition of a Riemann problem fulfills:* $U_L = U_R$ *and* $P_L = P_R$*, then, intermediate states in Godunov scheme and VFRoe-ncv scheme agree with:*

$$\begin{array}{l} U((x - x_{LR})/t = 0) = U_l = U_r = U_L = U_R \\ P((x - x_{LR})/t = 0) = P_l = P_r = P_L = P_R \end{array} \tag{4.4}$$

where x_{LR} *stands for the position of the initial interface between cells* L, R.

The proof is well known for Godunov scheme, and straightforward for the VFRoe-ncv scheme.

PROPERTY 4.3. *For given initial data in agreement with:* $U_k^n = U_0$ *and* $p_k^n = P_0$ *with* $k = i-1, i, i+1$*, both schemes ensure that:* $U_i^{n+1} = U_0$.

5. Behaviour of Godunov type schemes with EOS in T_1. In addition to property 4.3, we have:

PROPERTY 5.1. *For given EOS in* T_1*, and for given initial data in agreement with:* $U_k^n = U_0$ *and* $p_k^n = P_0$ *with* $k = i-1, i, i+1$*, above mentionned schemes also ensure that:*

$$p_i^{n+1} = P(\rho_i^{n+1}, e_i^{n+1}, C_i^{n+1}, \psi_i^{n+1}) = P_0 \tag{5.1}$$

Thus these schemes perfectly preserve unsteady contact discontinuities when restricting to EOS in T_1.

6. Behaviour of Godunov type schemes with EOS in T_2 or T_3. If we still use previous definition $p_i^{n+1} = P_i^{n+1}$, where $P_i^{n+1} = P(\rho_i^{n+1}, e_i^{n+1}, C_i^{n+1}, \psi_i^{n+1})$, as defined in (1.2), property 5.1 mentionned above is violated here. We first give here some results obtained using EOS in T_2 as follows: $\rho e = P/(\gamma(C) - 1)$ where $\gamma(C) = 1,4C+5,5(1-C)$. This corresponds to some stiffened gas EOS (with $P_\infty = 0$). Initial conditions are such that both U and P should remain constant w.r.t. time and space. Results presented below (Figures 6.1, 6.2) correspond to standard "first-order" VFRoe-ncv scheme, using CFL number 0.5, and regular meshes containing 400 nodes (coarse mesh though "fine" industrial mesh when considering the "3-D counterpart") and 40000 nodes (fine mesh). Note that the relative error in L^∞ norm is approximately around 30 % on the coarse mesh. The latter diminishes when refining the mesh, and is about 5 % on the finest mesh. The numerical method nevertheless converges (in L^1 norm) towards the right solution when the mesh size is refined.

We turn now to EOS in T_3, focusing on Van der Waals EOS. Once more, property 5.1 mentionned above is violated when using P_i^n to initialize interface Riemann problems. We still emphasize that the basic first order conservative numerical method (exact Godunov or) VFRoe-ncv nonetheless provides convergent approximations of

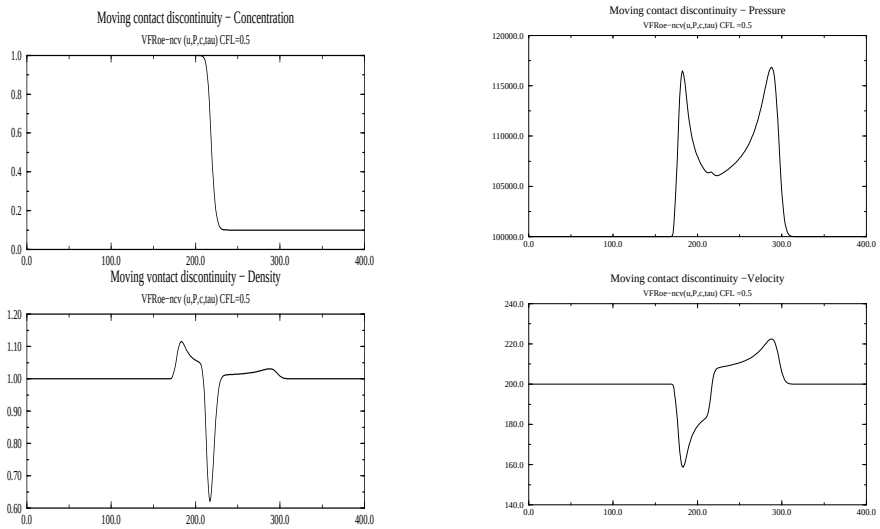

FIG. 6.1. *Moving contact discontinuity on coarse mesh*

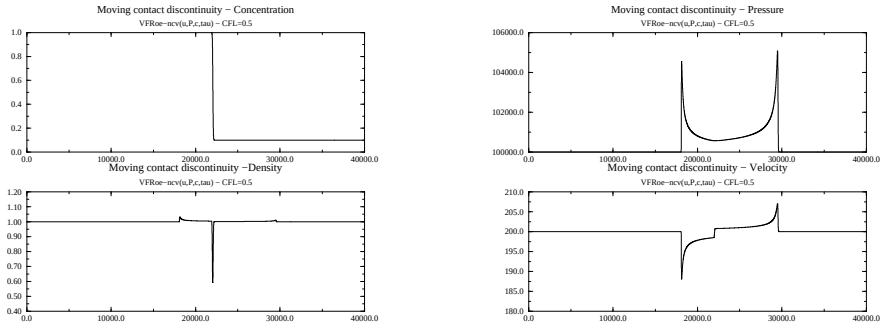

FIG. 6.2. *Moving contact discontinuity on fine mesh*

the solution. Figure 6.3 shows the behaviour of the L^1 error norm for both pressure and velocity variables, considering the first order scheme, with $CFL = 0.5$, and uniform meshes with 200 cells up to 20000 cells. Initial conditions are simply:

$$U_L = U_R = 100, \quad \rho_L = 100, \quad C_L = C_R = 1,$$
$$P_L = P_R = 10^6, \quad \rho_R = 200, \quad \psi_L = \psi_R = 1.$$

The rate of convergence is clearly $\frac{1}{2}$ as expected (since contact discontinuities are not perfectly preserved). However the very poor accuracy on coarse meshes is not

appealing for industrial purposes.

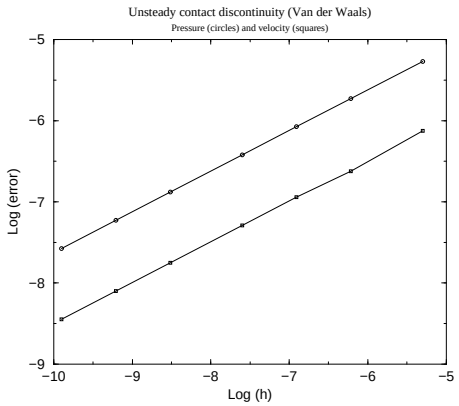

FIG. 6.3. *L1 error norm*

7. Hybrid version of Godunov-type schemes applied to $T_2 \cup T_3$.

7.1. Basic idea. We now decompose any EOS in terms of EOS in $T_1 \cup T_2$ and the remaining part, thus:

$$\begin{array}{c} \phi_3(P,\rho,C,\psi) = \rho e - \phi_1(P,\rho,C,\psi) - \phi_2(P,C,\psi) \\ \phi_1(P,\rho,C,\psi) = \rho(a_1(P) + b_1(P)C + c_1(P)\psi) + d_1(P) \\ \phi_2(P,C,\psi) = f_2(C,\psi)h_2(P) + g_2(C,\psi) \end{array} \tag{7.1}$$

The decomposition should be achieved in order to "minimize" contributions in $T_2 \cup T_3$. Hence, we define $a_1(P)$, $b_1(P)$, $c_1(P)$, $d_1(P)$ first, and then introduce $f_2(C,\psi)$, $g_2(C,\psi)$ and $h_2(P)$ in order to "minimize" the residual part $\phi_3(P,\rho,C,\psi)$. This is achieved in practice in a natural way when focusing on analytic laws such as those imbeded in mixture of perfect gases, stiffened gas EOS, Van der Waals EOS, Chemkin database, Tamman EOS and many other laws such as those used to construct thermodynamical tables. For given value of constant P_{ref}, we also introduce the function:

$$g_0(C,\psi) = f_2(C,\psi)h_2(P_{ref}) + g_2(C,\psi) \tag{7.2}$$

The latter quantity is governed by the following *redundent* equation when no discontinuity is present in the field:

$$\frac{\partial g_0(C,\psi)}{\partial t} + U\frac{\partial g_0(C,\psi)}{\partial x} = 0 \tag{7.3}$$

or alternatively by:

$$\frac{\partial \rho g_0(C,\psi)}{\partial t} + \frac{\partial (\rho g_0(C,\psi))U}{\partial x} = 0 \tag{7.4}$$

We note that this conservative formulation is "valid" if additional jump relations provided by the latter are fulfilled by natural jump relations recalled above. We note that the associated suggested jump relation is:

$$-\sigma[\rho g_0(C,\psi)] + [\rho g_0(C,\psi)U] = 0 \tag{7.5}$$

When combined with (true) jump relation associated with mass conservation this provides:

$$\overline{\rho v}[g_0(C,\psi)] = 0 \quad \text{and} \quad v = U - \sigma \tag{7.6}$$

When v is null (contact discontinuity), the latter is ensured of course. Besides, in Genuinely Non Linear 1 and 5 fields, $\overline{\rho v}$ is non zero but $g_0(C,\psi)$ is constant, hence the assertion holds. We underline that this "true" conservative form is specific to EOS in T_2. We emphasize anyway that we will not use the "conservation law" for $\rho g_0(C,\psi)$, since the latter does not correspond to any physically conserved quantity. Moreover, Abgrall analysis has confirmed that this quantity is not the adequate variable to propagate.

For regular solutions of the basic five equation model, the *redundent* governing equation for ϕ_3 is simply:

$$\frac{\partial}{\partial t}\phi_3(P,\rho,C,\psi) + U\frac{\partial}{\partial x}\phi_3(P,\rho,C,\psi) + \Big(\hat{\gamma}P\frac{\partial \phi_3}{\partial P} + \rho\frac{\partial \phi_3}{\partial \rho}\Big)\frac{\partial U}{\partial x} = 0 \tag{7.7}$$

which of course may degenerate if $\phi_3 = 0$. Unlike when dealing with EOS in T_2, one cannot provide a conservative re-formulation of the latter which enables to retrieve the true jump conditions. We may thus expect some greater difficulties when attempting to compute the extra non conservative governing equation for ϕ_3 [24].

Focus for instance on Van der Waals EOS, then:

$$\left\{\begin{array}{l} \rho e = \phi_1(P,\rho,C,\psi) + \phi_2(P,C,\psi) + \phi_3(P,\rho,C,\psi), \\ \phi_1(P,\rho,C,\psi) = \frac{(1-b\rho)P}{\gamma-1}, \\ \phi_2(P,C,\psi) = 0, \\ \phi_3(P,\rho,C,\psi) = a\rho^2(\frac{-b\rho}{\gamma-1} + \frac{2-\gamma}{\gamma-1}). \end{array}\right.$$

Obviously in this particular case, the function g_0 is null.

7.2. Numerical scheme. The basic scheme is the following *for any EOS*:

$$\left\{\begin{array}{lll} h_i\big(W_i^{n+1} - W_i^n\big) & + \delta t\big(F(\Psi(Y^*_{i+1/2})) - F(\Psi(Y^*_{i-1/2}))\big) = 0, \\ h_i\big((g_0)_i^{n+1} - (g_0)_i^n\big) & + \delta t\hat{U}_i\big((g_0)^*_{i+1/2} - (g_0)^*_{i-1/2}\big) = 0, \\ h_i\big((\phi_3)_i^{n+1} - (\phi_3)_i^n\big) & + \delta t\hat{U}_i\big((\phi_3)^*_{i+1/2} - (\phi_3)^*_{i-1/2}\big) \\ & + \delta t\hat{H}_i\big(U^*_{i+1/2} - U^*_{i-1/2}\big) = 0, \end{array}\right.$$

with

$$2\hat{U}_i = U^*_{i+1/2} + U^*_{i-1/2},$$
$$2\hat{H}_i = (\hat{\gamma}P\frac{\partial \phi_3}{\partial P} + \rho\frac{\partial \phi_3}{\partial \rho})^*_{i-1/2} + (\hat{\gamma}P\frac{\partial \phi_3}{\partial P} + \rho\frac{\partial \phi_3}{\partial \rho})^*_{i+1/2}.$$

The definition of the numerical flux is now the following:

$$F(W^*) = \left(\rho^*U^*, \rho^*U^*C^*, \rho^*U^*U^* + P^*, U^*(\frac{\rho^*(U^*)^2}{2} + P^*) + U^*(\rho e)^*, \rho^*U^*\psi^*\right)$$

where $(\rho e)^* = \phi_1(P^*,\rho^*,C^*,\psi^*) + \phi_2(P^*,C^*,\psi^*) + \phi_3(P^*,\rho^*,C^*,\psi^*)$, $W^* = \Psi(Y^*)$ and $(g_0)^* = g_0(C^*,\psi^*)$. The series $(f_2)_i^k$ (respectively $(g_2)_i^k$) issues from computation

of g_0 setting $h_2(P_{ref}) = 0$ (respectively $h_2(P_{ref}) = 1$), and should not be confused with $f_2(C_i^k, \psi_i^k)$ (or $g_2(C_i^k, \psi_i^k)$ respectively).

The cell pressure used to compute the local Riemann problems at the beginning of the next time step namely:

$$p_i^{n+1} = \tilde{P}_i^{n+1}$$

is obtained by inverting:

$$\left\| \begin{array}{l} \text{Find } \tilde{P}_i^{n+1} \text{ solution of} \\ \rho_i^{n+1} e_i^{n+1} - ((g_2)_i^{n+1} + (\phi_3)_i^{n+1}) \end{array} \right. = \begin{array}{l} (f_2)_i^{n+1} h_2(\tilde{P}_i^{n+1}) \\ + \phi_1(\tilde{P}_i^{n+1}, \rho_i^{n+1}, C_i^{n+1}, \psi_i^{n+1}) \end{array}$$

where $\rho_i^{n+1} e_i^{n+1} = E_i^{n+1} - ((Q_i^{n+1})^2)/(2\rho_i^{n+1})$ and with given values E_i^{n+1}, Q_i^{n+1}, ρ_i^{n+1}, C_i^{n+1}, ψ_i^{n+1} provided by discrete conservative equations, and $(f_2)_i^{n+1}$, $(g_2)_i^{n+1}$, $(\phi_3)_i^{n+1}$ provided by discrete non-conservative equations.

7.3. Main property and remarks. We now have the main property:

PROPERTY 7.1. *For any EOS in $T_1 \cup T_2 \cup T_3$, and for given initial data in agreement with: $U_k^n = U_0$ and $p_k^n = P_0$ with $k = i-1, i, i+1$, the above mentionned scheme ensures that:*

$$p_i^{n+1} = P_0 \quad \textit{and} \quad U_i^{n+1} = U_0.$$

Remark. When considering the specific case of stiffened gas EOS, it is emphasized that the proposed scheme identifies with Abgrall and Saurel proposal [42], by setting $h_2(P) = P$ in $\phi_2(P, C, \psi)$.

Remark. Actually, there is no proof whether the hybrid scheme converges, and assuming it does, there is little evidence that it converges towards the right weak solution (which is perfectly and uniquely defined) when discontinuities are present in the computational field, owing to the non conservative form of the whole scheme. This will be discussed further on.

Remark. We first note that the frame of EOS which lie exactly in T_1 is contained in the global formulation above since in that case, both ϕ_2 and ϕ_3 are null, and as a result P_i^{n+1} is computed as ($\phi_1 = \rho e$):

$$\left\| \begin{array}{l} \text{Find } P_i^{n+1} \text{ solution of} \\ \rho_i^{n+1} e_i^{n+1} = \phi_1(P_i^{n+1}, \rho_i^{n+1}, C_i^{n+1}, \psi_i^{n+1}) \end{array} \right.$$

and one retrieves the fully -standard- conservative scheme.

Remark. We have implicitely assumed that all EOS will have some non zero contribution in at least one class among T_1 or T_2. Otherwise updating the cell pressure through relation described above would be no longer feasable, and should be replaced by:

$$\left\| \begin{array}{l} \text{Find } \tilde{P}_i^{n+1} \text{ solution of} \\ (\phi_3)_i^{n+1} = \phi_3(\tilde{P}_i^{n+1}, \rho_i^{n+1}, C_i^{n+1}, \psi_i^{n+1}). \end{array} \right.$$

This frame is very unlikely to happen in practice, and all EOS considered herein which arise from the literature do have some contribution in $T_1 \cup T_2$. This academic case will nonetheless be examined in the last section.

Remark. We also obviously note that formally, both second and third non conservative discrete equations in (7.2) might be put together. This is due to the fact that:

$$\hat{\gamma} P \frac{\partial g_0}{\partial P} + \rho \frac{\partial g_0}{\partial \rho} = 0$$

and to the use of the superposition principle. We nonetheless will still distinguish both for at least two reasons. First, we have noted that EOS in T_2 is actually a specific case of EOS in the sense that "exact" conservative formulation of the governing equation of g_0 is available unlike with EOS with contributions in T_3. Second, we note that doing so (i.e. gathering both contributions) would result in an illposedness of value of P_i^{n+1} when precisely focusing on EOS in T_2. Last but not least, we will check that accuracy on very fine meshes may be slowed down when doing so (see section about the influence of the decomposition).

Remark. It must be underlined too that values of $(f_2)_i^n$ might be updated at the beginning of each time step using the computed values of C and ψ, that is $f_2(C_i^n, \psi_i^n)$. This seems appealing but it would result in a non conservative scheme for the governing equation of the total energy, if one still aims at perfectly preserving moving contact discontinuities. This alternative is thus disregarded hereafter.

Remark. From a numerical point of view, it is also necessary to point out that the numerical scheme which is used to compute governing equation of ϕ_3 is consistent with conservative equations for total mass and mass species. This means that for given laws of the form:

$$\phi_3(P, \rho, C, \psi) = \mu_0 \rho + \mu_1 \rho C + \mu_2 \rho \psi.$$

The discrete equation of ϕ_3 is exactly the counterpart of the linear combination of discrete equations of ρ and ρC. Though it would correspond to some "wrong" decomposition of the EOS - all these contributions should have been set in T_1 -, one nonetheless needs to examine this "virtual" case. Thus, in that particular case, it may be not only be rewritten in the form:

$$\frac{\partial \phi_3(P, \rho, C, \psi)}{\partial t} + \frac{\partial U \phi_3(P, \rho, C, \psi)}{\partial x} = 0$$

from a continuous point of view, but one notices that the discrete governing equation of ϕ_3 is also a linear combination of discrete equations of $\rho, \rho C, \rho\psi$, and thus retrieves the correct conservative form:

$$h_i((\phi_3)_i^{n+1} - (\phi_3)_i^n) + \delta t((U\phi_3)_{i+1/2}^* - (U\phi_3)_{i-1/2}^*) = 0.$$

The latter remark no longer holds when defining for instance $(\hat{H})_i = H_i^n$. Even more some counterpart of this discretization has been experienced before to provide loss of stability in other computations (computation of Reynolds stress closures in compressible turbulent flows).

¿From an industrial point of view, it does not seem compulsory to get the right $(\hat{H})_i$, more precisely the one which yields correct jump conditions. This will be checked *a posteriori* when computing Van der Waals EOS which is a good example where contribution in T_3 is not negligible when compared with contribution in T_1. It nonetheless seems appealing from an academic point of view, but it must be underlined that feasability in a one dimensional framework does not imply the counterpart in a three dimensional case.

8. Numerical results.

8.1. Stiffened gas EOS. Numerical results below are dedicated to simplified stiffened gas EOS in T_2 (since $(P_\infty)_1 = (P_\infty)_2 = 0$) as follows:

$$\rho e(P, \rho, C, \psi) = \frac{P}{\gamma(\psi) - 1}$$

where $\gamma(\psi) = 1,667\psi + 1,4(1-\psi)$. The decomposition is thus the following:

$$\left\{ \begin{array}{l} \rho e = \phi_2(P, C, \psi) = f_2(C, \psi) h_2(P) + g_2(C, \psi), \\ h_2(P) = P \ , \ f_2(C, \psi) = \frac{1}{\gamma(\psi)-1} \ , \ g_2(C, \psi) = \frac{P_\infty(\psi)}{\gamma(\psi)-1} \ , \\ (\phi_1(P, \rho, C, \psi) = \phi_3(P, \rho, C, \psi) = 0). \end{array} \right.$$

A first series of results corresponds to initial conditions proposed by Sandra Rouy [40]:

$$\begin{array}{llll} U_L = 0, & P_L = 120000, & \rho_L = 0.192, & \psi_L = 1, \\ U_R = 0, & P_R = 100000, & \rho_R = 1.156, & \psi_R = 0. \end{array}$$

Results presented below (figure 8.1) correspond to standard "first-order" VFRoe-ncv scheme, using CFL number 0.5, and regular meshes containing 100 nodes (coarsened mesh), and 40000 nodes (fine mesh). Results obtained with the hybrid version of the approximate Godunov scheme apparently converges towards the same solution when the mesh is refined. Nonetheless, the approximate solution on coarse mesh is indeed nicer when using the hybrid version described below.

We turn now to a simpler set of IC, as follows:

$$\begin{array}{llll} U_L = ((\frac{1}{\rho_R} - \frac{1}{\rho_2})(P_L - P_R))^{0.5}, & P_L = P_R \frac{\beta_R z - 1}{\beta_R - z}, & \rho_L = 4.0, & \psi_L = 1, \\ U_R = 0, & P_R = 100000, & \rho_R = 1.0, & \psi_R = 0, \end{array}$$

where $\beta_R = \frac{\gamma_2+1}{\gamma_2-1}$, and $z = \frac{\rho_2}{\rho_R}$ with $\rho_2 = 2$. This clearly results in a pure right going 3 shock. This Riemann problem is close to the previous one, since the difference lies in the ghost 1-wave here, which turned to be a rarefaction wave before. However, one may clearly expect that this regular wave cannot inhibit the convergence towards the right solution. In addition, present case enables to get rid of the compulsory error in the prediction of the regular 1- rarefaction wave, which might hide some defficiency of the hybrid scheme. In practice, the present IC require that the hybrid scheme manages computing the exact intermediate state of density on the right side of the -moving- contact discontinuity, which is not obvious at all. We have plot below the error using L^1 norm. Uniform meshes contain from 100 up to 160000 cells. The CFL number still equals 0.5. The error obviously vanishes as the mesh size tends towards zero (see figure 8.2). The rate of convergence for density is slightly greater than $\frac{1}{2}$, and the rate of convergence for U and P variables is 1. We emphasize that the rate is $\frac{1}{2}$ for ρ, U, P when using basic conservative scheme (figure 8.2).

8.2. Van der Waals EOS. Note that when restricting to Van der Waals EOS, there is no need to compute redundent information for (null) function g_0. We will indeed compute "twice" an approximation of the density when focusing on Van der Waals EOS. Constants used in the EOS are: $a = 1684.54$, $b = 0.001692$, $R = 461.5$,

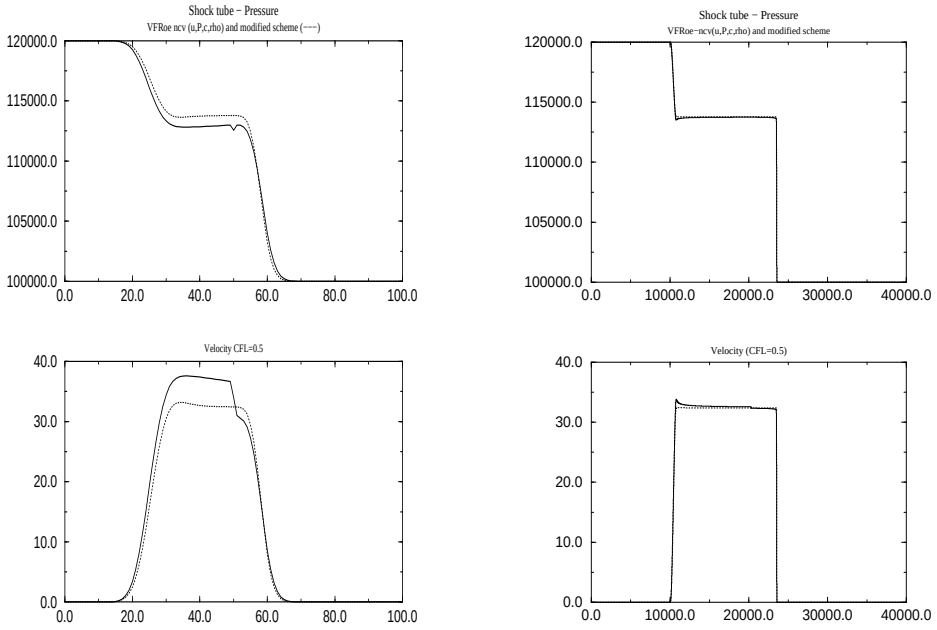

FIG. 8.1. *Shock tube with EOS in T_2 - coarse mesh (left), fine mesh (right)*

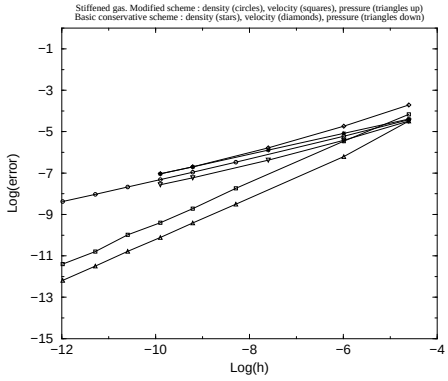

FIG. 8.2. *Pure unsteady 3-shock with EOS in T_2 - L1 error norm*

$C_v = 1401.88$. We recall below the decomposition:

$$\begin{cases} \rho e = \phi_1(P,\rho,C,\psi) + \phi_2(P,C,\psi) + \phi_3(P,\rho,C,\psi), \\ \phi_1(P,\rho,C,\psi) = \frac{(1-b\rho)P}{\gamma-1}, \\ \phi_2(P,C,\psi) = 0, \\ \phi_3(P,\rho,C,\psi) = a\rho^2(\frac{-b\rho}{\gamma-1} + \frac{2-\gamma}{\gamma-1}). \end{cases}$$

8.2.1. Shock tube case. We focus here on test case proposed by Letellier and Forestier [35]. Initial data is given by [35]:

$$\begin{array}{llll} U_L = 0, & P_L = 37311358, & \rho_L = 333, & C_L = 1, \\ U_R = 0, & P_R = 21770768, & \rho_R = 111, & C_R = 1. \end{array}$$

Figures 8.3, 8.4 refer to the comparison of both approximations provided by the basic fully conservative scheme and the hybrid scheme when computing a shock tube case on different meshes. Results are obviously more appealing on the latter when using hybrid version of the scheme. The L^1 error norm associated to the hybrid scheme is given on the last figure 8.5 of this series, as a function of the mesh size. We note that on the finest mesh, which is clearly out of reach of present computers for 3D calculations, the decrease of error slows down.

For seak of completeness, we now examine the remaining two configurations of the basic 1D Riemann problem, which either involve two shock waves or two rarefactions waves.

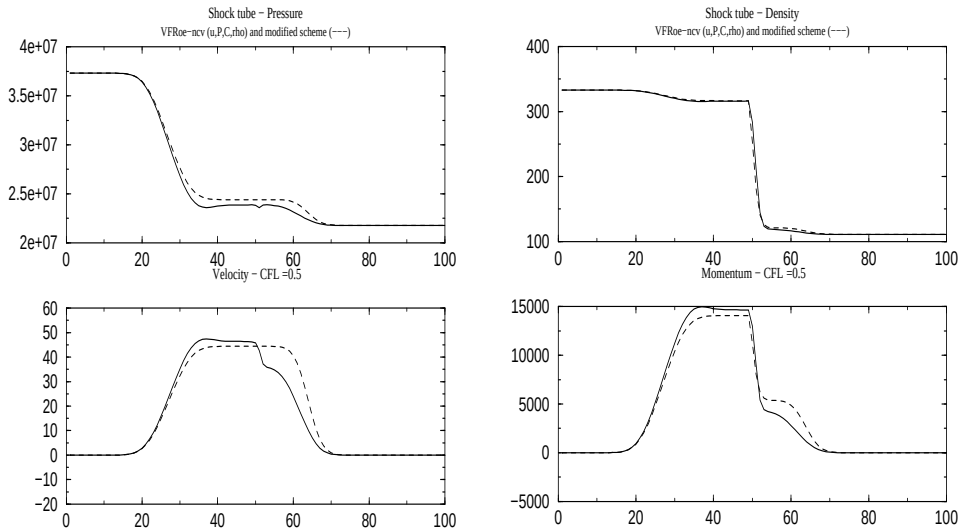

FIG. 8.3. *Shock tube with EOS in T_3 - coarse mesh*

8.2.2. Double rarefaction wave. We now examine some symmetrical double rarefaction wave. This enables to predict the behaviour of the scheme close to the wall boundary behind some bluff body, when applying for the mirror technique. Initial conditions are now:

$$\begin{array}{llll} U_L = -100, & P_L = 10^7, & \rho_L = 111, & C_L = \psi_L = 1, \\ U_R = 100, & P_R = 10^7, & \rho_R = 111, & C_R = \psi_R = 1. \end{array}$$

The time step is still in agreement with CFL condition $CFL = 0.5$. The mesh is composed of 200 regular cells. The first order version of the scheme has been used here (see figure 8.6-left). Note that the small glitch on the density at the initial position of the membrane is already present when using the standard Godunov scheme or VFRoe-ncv scheme in a fully conservative form. One might expect a rather nice behaviour of the scheme here since the exact solution contains no shock wave.

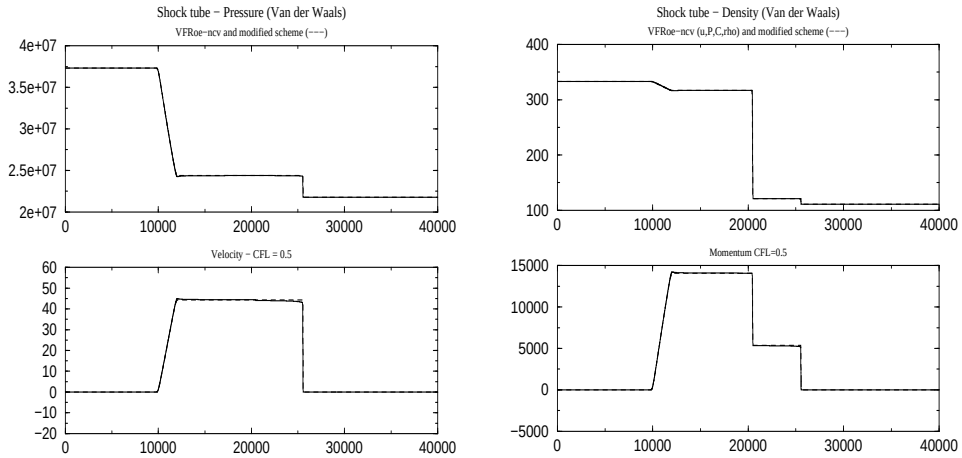

FIG. 8.4. *Shock tube with EOS in T_3 - finest mesh*

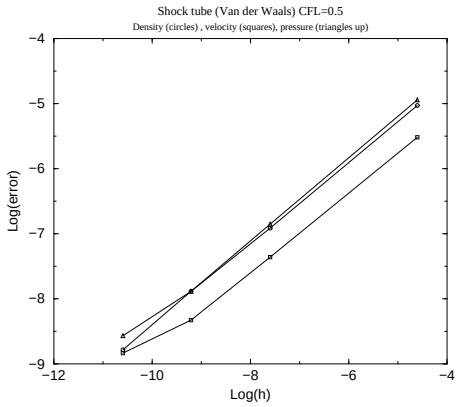

FIG. 8.5. *L1 error norm for hybrid scheme*

8.2.3. Double shock wave. Before going further on, we examine some symmetrical double shock wave. This provides an initial guess of what happens when the flow is impinging the wall boundary. Initial conditions are:

$$\begin{array}{llll} U_L = 100, & P_L = 10^7, & \rho_L = 111, & C_L = \psi_L = 1, \\ U_R = -100, & P_R = 10^7, & \rho_R = 111, & C_R = \psi_R = 1. \end{array}$$

The CFL number is the same as above. The mesh still contains two hundred nodes (see figure 8.6-right).

8.2.4. 3-shock waves. We eventually investigate some 3-shock waves. Recall that one advantage here is that the 1-wave will be a "ghost" wave, and therefore will generate a much smaller amount of error, which might hide deficiencies occuring in shock waves when focusing on the standard shock tube apparatus. Hence, we first introduce IC as follows:

$$\begin{array}{llll} U_L = U_R + ((\frac{1}{\rho_R} - \frac{1}{\rho_2})(P_L - P_R))^{0.5}, & & \rho_L = 4.0, & C_L = \psi_L = 1, \\ U_R = 0, & & \rho_R = 1.0, & C_R = \psi_R = 1, \end{array}$$

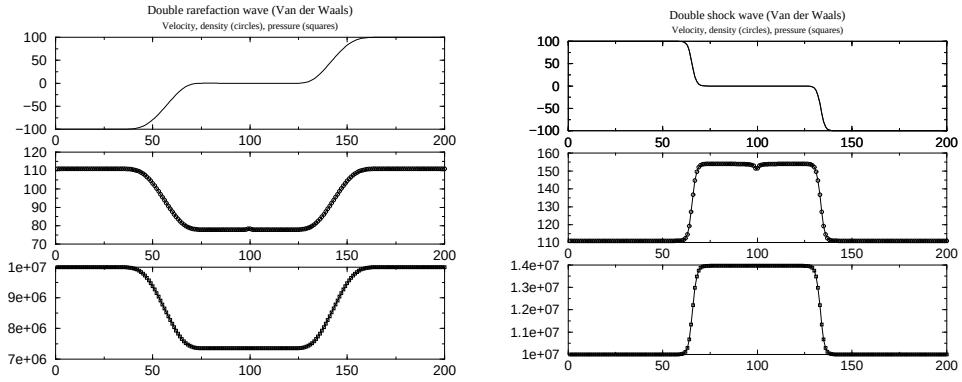

FIG. 8.6. *Double rarefaction wave (left) and double shock wave (right) with EOS in* T_3

with $P_R = 100000$, $\rho_2 = 2$ and $P_L > P_R$ solution of:

$$2\rho_2\rho_R(e(P_L,\rho_2) - e(P_R,\rho_R)) = (P_L + P_R)(\rho_2 - \rho_R).$$

Intermediate states indexed $1, 2$ agree with $U_L = U_1 = U_2$, $P_L = P_1 = P_2$, $\rho_L = \rho_1$.

The L^1 error norm is given on figure 8.7. The smaller mesh contains 160000 nodes and the coarser mesh 100 cells. For the whole range, the error norm of the density tends to 0 as $h^{1/2}$. We notice anyway, that the rate of convergence for both velocity and pressure is approximately 1 for meshes with 100 up to 10000 cells, but the error remains stationary (w.r.t. mesh size) for meshes containing more than ten thousand nodes. This obviously means that some -indeed small value- $O(1)$ error is present in the solution close to the 3-shock wave. An ambiguous point is that it may only be exhibited when using mesh refinement which involves much more cells than one may afford in practice, and which is also seldomly investigated by developers. The counterpart in a 3D framework would require more than 10^{12} cells. This implies in practice that the hybrid scheme should not be disregarded. We will come back to similar comments in a section below.

We turn now to different IC where densities and pressures are much higher:

$$\begin{array}{lll} U_L = U_R + ((\frac{1}{\rho_R} - \frac{1}{\rho_2})(P_L - P_R))^{0.5}, & \rho_L = 320.0, & C_L = \psi_L = 1, \\ U_R = 0, & \rho_R = 80.0, & C_R = \psi_R = 1, \end{array}$$

with $P_R = 8000000$, $\rho_2 = 160$ and $P_L > P_R$ solution of:

$$2\rho_2\rho_R(e(P_L,\rho_2) - e(P_R,\rho_R)) = (P_L + P_R)(\rho_2 - \rho_R).$$

We have plot here the L^1 error norm on figure 8.8. Similar comments as previous ones still hold here, and the rate of convergence for the conservative scheme is clearly $\frac{1}{2}$ for the density, the pressure and the velocity. This is due to the fact that the local amount of error around the contact discontinuity for pressure and velocity is so high that it inhibits rate 1 to be set. Once again, the error with the modified scheme becomes stationnary when meshes involve more than 10^4 cells.

Remark. In any case, it confirms that EOS in T_2 and EOS in T_3 should not be confused, at least from a theoretical point of view. The occurence of a true non conservative product $H(W)\partial_x U$ in the governing equation of ϕ_3 inhibits the convergence towards the right solution on very fine meshes. These results are in agreement with scalar results obtained by Hou and Le Floch [24].

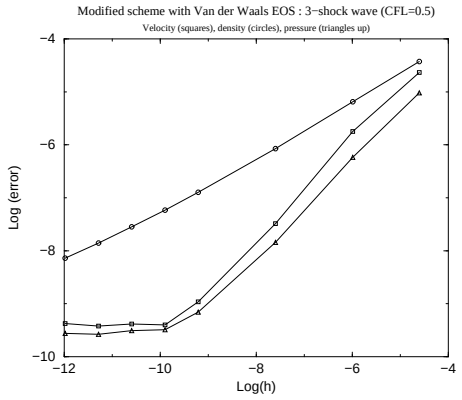

FIG. 8.7. *L1 error norm for hybrid scheme*

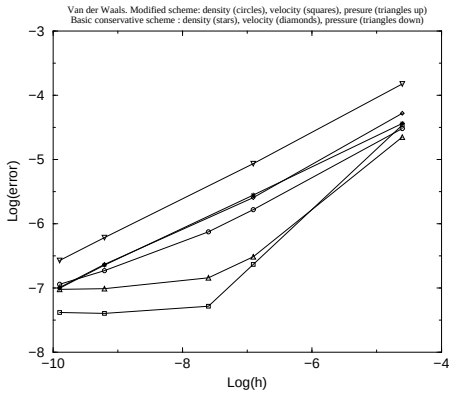

FIG. 8.8. *L1 error norm for conservative and hybrid scheme*

8.3. Chemkin database. We focus here on EOS provided in [32] and investigated in [10],[11]. The internal energy is a polynomial function in terms of the local temperature T.

$$\begin{cases} \rho e = r\mu_0\rho + (\mu_1 - 1)P + \sum_{2\leq n\leq k} \mu_n \frac{P^n}{(r\rho)^{n-1}}, \\ P = r\rho T. \end{cases}$$

Straightforward decomposition yields:

$$\begin{cases} \rho e = \phi_1(\rho, P, C, \psi) + \phi_2(P, C, \psi) + \phi_3(\rho, P, C, \psi), \\ \phi_1(\rho, P, C, \psi) = r\mu_0\rho + (\mu_1 - 1)P, \\ \phi_2(P, C, \psi) = 0, \\ \phi_3(\rho, P, C, \psi) = \sum_{2\leq n\leq k} \mu_n \frac{P^n}{(r\rho)^{n-1}}. \end{cases}$$

We may simply compute the speed of acoustic waves as:

$$c^2 = \frac{\hat{\gamma}P}{\rho} = rT\frac{\mu_1 + \sum_{2\leq n\leq k} n\mu_n T^{n-1}}{\mu_1 - 1 + \sum_{2\leq n\leq k} n\mu_n T^{n-1}}.$$

The whole algorithm only requires updating the cell pressure $p_i^{n+1} = \tilde{P}_i^{n+1}$ at the end of the time step as follows:

$$\tilde{P}_i^{n+1} = \frac{(\rho e)_i^{n+1} - \mu_0 r(\rho)_i^{n+1} - (\phi_3)_i^{n+1}}{\mu_1 - 1}.$$

Remark. Note that unlike when using the basic Godunov or VFRoe-ncv schemes, this only requires an algebraic manipulation and does not require any Newton procedure to compute P_i^{n+1} in each cell as a solution of:

$$(\rho e)(P_i^{n+1}, \rho_i^{n+1}) = E_i^{n+1} - \frac{Q_i^{n+1}Q_i^{n+1}}{(2\rho)_i^{n+1}}$$

which results in a great decrease of the computational CPU time.

We refer to [11] which provides data of IC used herein. The latter computations (figure 8.9) have been obtained using present approximate Godunov scheme VFRoe-ncv with (τ, U, P) variable. Other computations with help of Roe approximate Riemann solver are given in [12]. Details concerning entropy are briefly recalled in appendix B of [19].

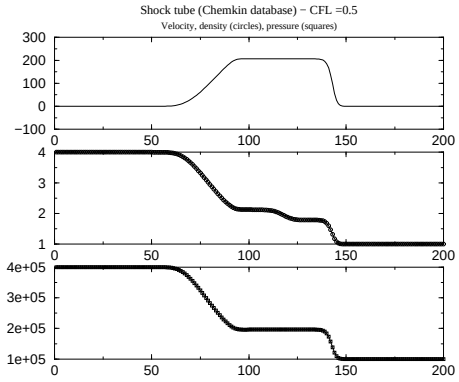

FIG. 8.9. *Shock tube using Chemkin database - coarse mesh*

8.4. Tabulated EOS. For arbitrary non analytic EOS, we now define the decomposition of the EOS in the class T_1 and T_3. This may be achieved defining some function $d_1(P) = \frac{P}{\gamma_1 - 1}$, which is close enough to the real state law. The constant γ_1 is computed introducing some least square minimization process.

$$\left\{ \begin{array}{l} \phi_1(\rho, P, C, \psi) = \frac{P}{\gamma_1 - 1}, \\ \phi_2(\rho, C, \psi) = 0, \\ \phi_3(\rho, P, C, \psi) = \rho e - \frac{P}{\gamma_1 - 1}. \end{array} \right.$$

Thus the redundent equation which is computed reads:

$$\frac{\partial}{\partial t}\phi_3(P, \rho, C, \psi) + U\frac{\partial}{\partial x}\phi_3(P, \rho, C, \psi) + \Big(\rho e + P - \frac{\gamma P}{\gamma_1 - 1}\Big)\frac{\partial U}{\partial x} = 0.$$

8.4.1. Influence of decomposition. We examine very briefly below whether some discrepancy in the decomposition implies some loss of accuracy, or in other words try to evaluate the stability of the overall method w.r.t. to the choice of the decomposition. Assume for instance that the real EOS reads: $(\rho e) = \frac{P}{\gamma_1 - 1}$. Imagine that some -on purpose- error occurs in the process in such a way that the decomposition yields:

$$\left\{ \begin{array}{l} \phi_1(\rho, P, C, \psi) = \frac{P}{\gamma_2 - 1}, \\ \phi_2(\rho, C, \psi) = 0, \\ \phi_3(\rho, P, C, \psi) = P(\frac{1}{\gamma_1 - 1} - \frac{1}{\gamma_2 - 1}), \end{array} \right.$$

where of course both constants are distinct. Despite from its simplicity, we first note that the resulting hybrid scheme does not compute the same approximation of the internal energy than the fully conservative scheme.

8.4.2. Approximate decomposition. We set here $\epsilon = 0.1$ and:

$$\left\{ \begin{array}{l} \phi_1(\rho, P, C, \psi) = (1 - \epsilon)\frac{P}{\gamma_1 - 1}, \\ \phi_3(\rho, P, C, \psi) = \epsilon\frac{P}{\gamma_1 - 1}. \end{array} \right.$$

When focusing on the standard Sod shock tube problem which involves one 3-shock wave, and using meshes with up to 40000 nodes, the L^1 error norm has been plotted

on figure 8.10. While linear rate of convergence is achieved when using the correct decomposition (velocity (squares), pressure (triangles up), density (circles)), and thus the fully unmodified conservative scheme (see also [18]), the measured error associated to the hybrid scheme (velocity (diamonds), pressure (triangles down), density (stars)) diminishes much slower on finer meshes. Actually, detailed qualitative investigation around the numerical shock locations shows that both are separated by an $O(1)$ length, which can hardly be seen unless the mesh contains more than 10000 nodes, which is seldomly examined in pratice of course. This result confirms investigation of EOS in T_3 (Van der Waals) described previously. This is also confirmed in a "continuous" way by the next numerical experiment.

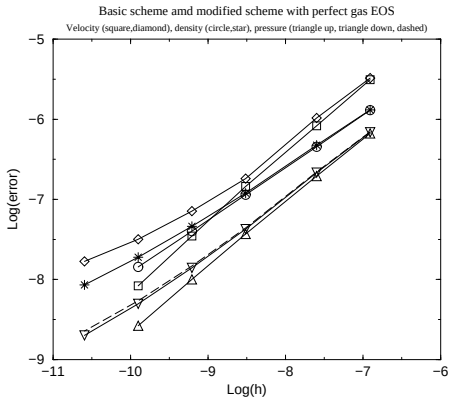

FIG. 8.10. *Perfect gas EOS: approximate decomposition*

8.4.3. Wrong decomposition. We set here $\epsilon = 1$, thus:

$$\phi_1 = 0 \quad \text{and} \quad \phi_3 = \frac{P}{\gamma_1 - 1}.$$

Updating the cell pressure at the end of the time step is performed through:

$$P_i^{n+1} = (\gamma_1 - 1)(\phi_3)_i^{n+1}.$$

We provide below some comparison of both approximations, using a coarse mesh with two hundred nodes and a fine mesh with 10000 nodes. It obviously appears that the hybrid scheme no longer converges towards the correct solution. Actually zooming the approximate solution provided by schemes with 5000 and 10000 cells enables to check that the number of nodes between the two locations of 3 shock waves doubles when refining the mesh by two. This is confirmed by computations on finer meshes. Of course the error still seems to be negligible on coarse meshes ! Results are here in agreement with [24].

9. A blend scheme. We eventually propose the following overall strategy, which relies on tuning of both the original conservative scheme to deal with fine meshes, and the above mentionned scheme to benefit from pure representation of moving contact discontinuities on coarse meshes. It simply requires some parametric function in order to switch from one scheme to the other when the mesh is refined, and of course when complex EOS are considered. Thus, the cell pressure which will be used in practice

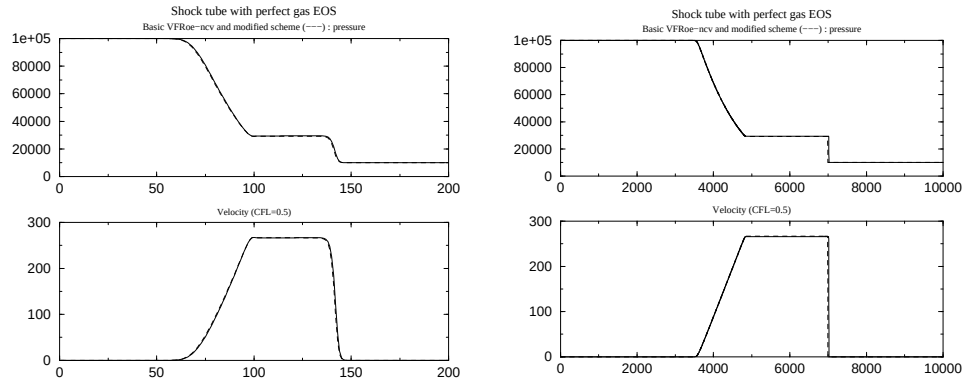

FIG. 8.11. *Perfect gas EOS: correct and wrong decomposition - coarse (left) and fine mesh (right)*

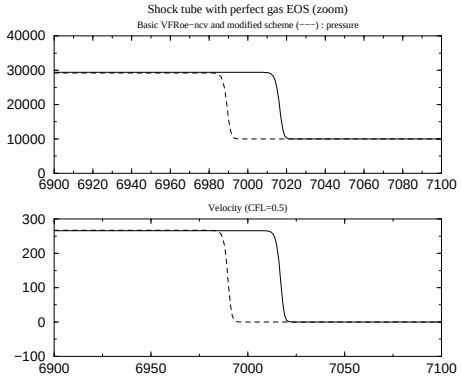

FIG. 8.12. *Perfect gas EOS: correct and wrong decomposition - finer mesh (zoom)*

will be p_i^{n+1}:

$$P_i^{n+1} = P(\rho_i^{n+1}, e_i^{n+1}, C_i^{n+1}, \psi_i^{n+1}),$$
$$p_i^{n+1} = \alpha(h) P_i^{n+1} + (1-\alpha(h))\tilde{P}_i^{n+1}.$$

where $\tilde{P}_i^n$ is given in a previous section, and h stands for the mean mesh size. For given EOS which do not have a contribution in T_3, $\alpha(h) = 1$ for EOS in T_1, and $\alpha(h) = 0$ if the contribution in T_2 is non vanishing. Otherwise, if the EOS is not in $T_1 \cup T_2$, $\alpha(h)$ should comply with:

$$\begin{cases} \alpha(h) = 1 \text{ if } h \leq h_0, \\ \alpha(h) = 0 \text{ if } h \geq h_1, \end{cases}$$

for given mesh sizes $h_0 < h_1$ provided by user.

In practice, standard conservative schemes correspond to the formal choice $h_0 = h_1 = +\infty$, whereas the so-called hybrid scheme corresponds to $h_0 = h_1 = 0$. Numerical tests reported above suggest some pratical values. The above blended scheme seems to represent some useful compromise in order to satisfy both mathematicians and those involved in solving industrial problems.

10. Conclusion. This paper was devoted to the computation of Euler type schemes with arbitrary equation of state, assuming the internal energy depends on

pressure and density variables, but also on concentrations of some species and a colour function. It has been shown that when focusing on exact or adequate approximate Godunov solvers, one needs to distinguish three different classes of EOS. One thus needs to compute some redundent information (from a continuous point) in order to cope with second and third classes. Actually, one needs first to decompose the internal energy in three terms which respectively belong to the latter three classes. Afterwards, one needs to compute an extra (respectively two) equation(s) when some contribution occurs in the second or third class (respectively in both second and third class) in the decomposition.

Some schemes have been proposed to compute the latter non conservative governing equations in addition to the first five conservative equations associated with total mass, mass of species, total momentum, total energy and colour function. Thus pure unsteady contact discontinuities are very well predicted on coarse meshes when using the so called hybrid scheme. Numerical results seem to confirm that the hybrid scheme permits more accurate computations *on coarse meshes* of shock tube experiments involving sharp contact discontinuities when focusing on a mixture of perfect gases, stiffened gas EOS or Van der Waals EOS. This is true for the vicinity of the contact discontinuity, but also around the connection of the end of the 1-rarefaction wave and the beginning of the 5-rarefaction wave. Discrete L^1 measure of convergence confirms convergence towards the right solution in some specific cases when the EOS has no contribution in T_3. Actually measurement of rate of convergence exhibits that both U, P converge as h towards the right solution, while concentration or density converge as $h^{\frac{1}{2}}$. Nonetheless, when refining *much* meshes, it clearly appears in some cases *involving contribution of the EOS in the third class* T_3, that, as might have been expected [24], the measure of convergence towards the correct solution is no longer in favour of the hybrid scheme when shocks are involved in computations. Numerical evidence shows that U, P still converge as h towards the right solution on coarse meshes (involving from 100 up to 20000 cells), but that the error then becomes stationary with respect to mesh size. This motivates the use of the blend scheme which benefits from nice approximations on coarse meshes of the hybrid scheme, and still inherits the property of convergence towards the right solution on finer meshes. In practice, this will in fact correspond to the use of the hybrid scheme since very few meshes contain more than $(10^2)^3$ cells in an industrial computation and none contains more than $(2.10^4)^3$ cells! The hybrid scheme is thus appealing for industrial purposes since it not only enables to increase accuracy on given (coarse) mesh size, but also enables to reduce CPU time due to the fact that computation of pressure is usually much faster when computing modified pressure $\tilde{P}$ rather than standard value $P(\rho_i^n, e_i^n, C_i^n, \psi_i^n)$. This is actually the case when applying Chemkin database, which only requires an algebraic calculus instead of a Newton procedure to compute cell pressure at the end of time step, but also when dealing with more complex EOS or tabulated EOS as suggested. It is emphasised that this remark takes into account the fact that two additional discrete equations for redundent information must be computed ; note that all interface information has already been prepared in the initial version of the algorithm, which obviously explains that the balance in CPU time is favourable to the hybrid scheme. Eventually, it seems to us that this work is not only useful in the framework of two-phase flow modelling with help of single fluid models of the Euler type, but also when retaining the two-fluid two-pressure approach.

Acknowledgments. The third author has been supported by Electricité de France (EDF) grant under contract C02770/ AEE2704. Computational facilities were

provided by EDF-Division Recherche et Développement.

Appendix. VFRoe-ncv schemes for systems of conservation laws. This appendix presents the construction a VFRoe-ncv schemes, focusing on systems of conservation laws. We reduce to the one dimensional case, with regular meshes (the extension to the multidimensional case and to unstructured meshes is classical). Following notations introduced in the body of the present paper, we denote W: $\mathbb{R}_+ \times \mathbb{R} \to \mathbb{R}^n$ the exact solution of the non degenerate hyperbolic system:

$$\left\{ \begin{array}{l} \dfrac{\partial W}{\partial t} + \dfrac{\partial F(W)}{\partial x} = 0, \\ W(0,x) = W_0(x). \end{array} \right.$$

Let Φ be a regular invertible function from $\mathbb{R}^n$ to $\mathbb{R}^n$ and Ψ its inverse. If W is a regular solution of the above system, then $Y = \Phi(W)$ is solution of

$$\frac{\partial Y}{\partial t} + B(Y)\frac{\partial Y}{\partial x} = 0$$

where $B(Y) = (D\Psi(Y))^{-1}(DF(\Psi(Y)))(D\Psi(Y))$.

As mentionned above, VFRoe-ncv schemes are approximate Godunov schemes. Hence, they may be written under the form

$$h_i(W_i^{n+1} - W_i^n) + \delta t(F(\Psi(Y^*_{i+1/2})) - F(\Psi(Y^*_{i-1/2}))) = 0.$$

We describe now the computation of $Y^*_{i+1/2}$. The state $Y^*_{i+1/2}$ corresponds to the exact solution Y^* at $x = 0$ of the linearized hyperbolic system:

$$\left\{ \begin{array}{l} \dfrac{\partial Y^*}{\partial t} + B(\hat{Y})\dfrac{\partial Y^*}{\partial x} = 0, \\ Y^*(0,x) = \left\{ \begin{array}{ll} Y_L = \Phi(W_i^n) & \text{if } x < 0, \\ Y_R = \Phi(W_{i+1}^n) & \text{if } x > 0, \end{array} \right. \end{array} \right.$$

where $\hat{Y} = (Y_L + Y_R)/2$. Since Y^* is the solution of a linear system, its computation is classical:

$$\begin{aligned} Y^*\left(\frac{x}{t}; Y_L, Y_R\right) &= Y_L + \sum_{\frac{x}{t} > \widetilde{\lambda_k}} ({}^t\widetilde{l_k}.(Y_R - Y_L))\widetilde{r_k}, \\ &= Y_R - \sum_{\frac{x}{t} < \widetilde{\lambda_k}} ({}^t\widetilde{l_k}.(Y_R - Y_L))\widetilde{r_k}, \end{aligned}$$

where $\widetilde{l_k}$, $\widetilde{\lambda_k}$ and $\widetilde{r_k}$, $k = 1, ..., n$, are respectively left eigenvectors, eigenvalues and right eigenvectors of matrix $B(\hat{Y})$. Thus, we have

$$Y^*_{i+1/2} = Y^*(0; Y_L, Y_R).$$

REFERENCES

[1] R. Abgrall, How to prevent pressure oscillations in multicomponent flow calculations: a quasi conservative approach, *J. Comp. Phys.*, 1995, vol. 125, pp. 150–160.

[2] R. Abgrall and S. Karni, Computations of compressible multifluids, *J. Comp. Phys.*, 2001, vol. 169, pp. 594–623.

[3] G. Allaire, S. Clerc and S. Kokh, A five equation model for simulating two phase flows with interfaces, *submitted for publication*.
[4] ———, A five equation model for the numerical solution of interfaces in two phase flows, *C. R. Acad. Sci. Paris*, 2000, vol. I-331, pp. 1017–1022.
[5] T. Barberon, P. Helluy and S. Rouy, Godunov schemes and multifluid flows, *in preparation*, 2001.
[6] M. Barret, E. Faucher and J.M. Hérard, Some schemes to compute flashing flows, *AIAA journal*, Vol. 40-4, 2002.
[7] S. Bilicki and D. Kardas, Approximation of thermodynamic properties for subcooled water and superheated steam, *Polish Academy of Sciences*, 1991.
[8] S. Bilicki and J. Kestin, Physical aspects of the relaxation model in two phase flows, *Proc. of the Royal Soc. of London*, 1990, vol. A428, pp. 379–397.
[9] S. Bilicki, J. Kestin and M.M. Pratt, A reinterpretation of the results of the moby dick experiments in terms of the non equilibrium model, *J. of Fluid Eng.*, 1990, vol. 112, pp. 212–217.
[10] T. Buffard, T. Gallouët and J.M. Hérard, *Schéma VFRoe en variables caractéristiques. Principe de base et applications aux gaz réels*, EDF-DER Report HE-41/96/041/A, 1996. In French.
[11] ———, A sequel to a rough Godunov scheme. Application to real gas flows, *Computers and Fluids*, 2000, vol. 29-7, pp. 813–847.
[12] M. Buffat and A. Page, *Extension of Roe's solver for multi species real gases*, Ecole Centrale de Lyon, Lyon, France Report LMFA report, 1995.
[13] S. Clerc, Accurate computation of contact discontinuities in flows with general equations of state, *Comp. Meth. in Applied Mech. and Eng.*, 1999, vol. 178, p. 245–255.
[14] ———, Numerical simulation of the homogeneous equilibrium model for two phase flows, *J. Comp. Phys.*, 2000, vol. 161-1, pp. 354–375.
[15] F. Coquel and B. Perthame, Relaxation of energy and approximate Riemann solvers for general pressure laws in fluid dynamics equations, *SIAM J. Numer. Anal.*, 1998, vol. 35-6, pp. 2223–2249. In Memory of Ami Harten.
[16] E. Faucher, J.M. Hérard, M. Barret and C. Toulemonde, Computation of flashing flows in variable cross-section ducts, *Int. J. of Comp. Fluid Dyn.*, 2000, vol. 13-3, pp. 365–391.
[17] R.P. Fedkiw, T. Aslam, B. Merriman and S. Osher, A non oscillatory eulerian approach to interfaces in multimaterial flows (the ghost fluid approach), *J. Comp. Phys.*, 1999, vol. 152, p. 457.
[18] T. Gallouët, J.M. Hérard and N. Seguin, *Some recent Finite Volume schemes to compute Euler equations using real gas EOS*, LATP Report 00-021, Université de Provence, France, 2000, *to appear in Int. J. for Num. Meth. in Fluids*.
[19] ———, *An hybrid scheme to compute contact discontinuities in Euler systems*, LATP Report 01-027, Université de Provence, France, 2001.
[20] ———, On the use of some symmetrizing variables to deal with vacuum, *submitted for publication*, 2002.
[21] S. Gavrilyuk and R. Saurel, Mathematical and numerical modelling of two phase compressible flows with inertia, *J. Comp. Phys.*, 2002, vol. 175, p. 326–360.
[22] E. Godlewski and P.A. Raviart, *Numerical approximation for hyperbolic systems of conservation laws*, Springer Verlag, 1996.
[23] S.K. Godunov, A difference method for numerical calculation of discontinous equations of hydrodynamics, *Sbornik*, 1959, pp. 271–300. In Russian.
[24] X. Hou and P. G. Le FLoch, Why non conservative schemes converge to wrong solutions, *Mathematics of computation*, 1994, vol. 62-206, pp. 497–530.
[25] A. In, Numerical evaluation of an energy relaxation method for inviscid real fluids, *SIAM J. Sci. Comp.*, 1999, vol. 21-1, pp. 340–365.
[26] ———, *Méthodes numériques pour les équations de la dynamique des gaz complexes et écoulements diphasiques*, PhD thesis, Université Paris VI, France, October 1999.
[27] M. Ishii, *Thermo-fluid dynamic theory of two-phase flows*, Collection de la Direction des Etudes et Recherches d'Electicité de France, 1975.
[28] A.K. Kapila, S.F. Son , J.B. Bdzil, R. Menikoff and D.S. Stewart, Two-phase modelling of DDT : structure of the velocity relaxation zone , *Physics of Fluids*, 1997, vol. 9(12), pp. 3885–3897.
[29] S. Karni, Multicomponent flow calculations by a consistent primitive algorithm, *J. Comp. Phys.*, 1994, vol. 112, pp. 31–43.
[30] ———, Hybrid multifluid algorithms, *SIAM J. Sci. Comp.*, 1996, vol. 17, pp. 1019–1039.
[31] S. Karni and R. Abgrall, Ghost fluid for the poor: a single fluid algorithm for multifluid,

Oberwolfach, 2001.
[32] R. Kee, J. Miller and T. Jefferson, *Chemkin: a general purpose, problem independant transportable fortran chemical kinetics code package*, SAND Report 80-8003, Sandia National Laboratories.
[33] S. Kokh, *Aspects numériques et théoriques de la modélisation des écoulements diphasiques compressibles par des méthosdes de capture d'interface*, PhD thesis, Université Paris VI, France, 2001.
[34] F. Lagoutiere, *Modélisation mathématique et résolution numérique de problèmes de fluides compressibles à plusieurs constituants*, PhD thesis, Université Paris VI, France, 2000.
[35] A. Letellier and A. Forestier, *Le problème de Riemann en fluide quelconque*, CEA-DMT Report 93/451, 1993. In French.
[36] R. LeVeque, *Numerical methods for conservation laws*, Birkhauser, 1992.
[37] R. Pollak, *Die thermodynamischen eigenschaften von wasser dargestellt durch eine kanonische zustands gleichung fur die fluiden homogenen und heterogenen zustande bis 1200 Kelvin und 3000 bars*, PhD thesis, Ruhr Universitat, Germany, 1974.
[38] P. Rascle and O. Morvant, *Interface utilisateur de Thetis - THErmodynamique en Tables d'InterpolationS*, EDF-DER Report HT-13/95021B, 1995. In French.
[39] P.L. Roe, Approximate Riemann solvers, parameter vectors and difference schemes, *J. Comp. Phys.*, 1981, vol. 43, pp. 357–372.
[40] S. Rouy, *Modélisation mathématique et numérique d'écoulements diphasiques compressibles*, PhD thesis, Université de Toulon et du Var, France, December 2000.
[41] R. Saurel and R. Abgrall, A multiphase godunov method for compressible multifluid and multiphase flows, *J. Comp. Phys.*, 1999, vol. 150, pp. 425–467.
[42] ———, A simple method for compressible multifluid flows, *SIAM J. Sci. Comp.*, 1999, vol. 21-3, pp. 1115–1145.
[43] J. Sethian, *Level set methods*, Cambridge University Press, 1996.
[44] K.M. Shyue, A fluid mixture type algorithm for compressible multicomponent flow with Van der Waals equation of state, *J. Comp. Phys.*, 1999, vol. 156, pp. 43–88.
[45] J. Smoller, *Shock waves and reaction diffusion equations*, Springer Verlag, 1983.
[46] E.F. Toro, *Riemann solvers and numerical methods for fluid dynamics*, Springer Verlag, 1997.
[47] I. Toumi, *Contribution à la modélisation numérique des écoulements diphasiques eau-vapeur*, Thèse d'habilitation, Université Paris Sud, France, 2000.